Geochimica et Cosmochimica Acta Vol. 56, pp. 4075–4090

0016-7037/92/$5.00 + .00

Apollo 15 green glass: Compositional distribution and petrogenesis

ALISON M. STEELE, RUSSELL O. COLSON, RANDY L. KOROTEV, and LARRY A. HASKIN
Department of Earth and Planetary Sciences, Box 1169, Washington University, 1 Brookings Drive, St Louis, MO 63130, USA

(*Received July* 30, 1991; *accepted in revised form May* 26, 1992)

Abstract—We have characterized a comprehensive suite of individual green-glass beads from Apollo 15 soil to determine interelement behavior and to constrain petrogenetic relationships. We analyzed 365 particles for trace elements by instrumental neutron activation analysis and analyzed 52 of them, selected to cover the compositional ranges observed for trace elements, for major elements by electron microprobe analysis. We confirm the observation of DELANO (1979) that the beads comprise discrete compositional groups, although two of the groups he defined are further split on the basis of trace-element compositions. Each of the resulting seven groups has distinct average rare-earth abundances. The coherence between major- and trace-element data was masked in previous studies by imprecision, correlated error, and nonrepresentative sampling of the different groups. Most of the compositional characteristics of the green glasses can be explained by a model for batch equilibrium melting of a nearly homogeneous, ultramafic source region, when the complicating effects of high pressure and low oxygen fugacity are taken into account. The previously puzzling behavior of Ni and Co as apparently incompatible elements may arise from partial reduction of those elements to the zero oxidation state, resulting in low mineral/melt partition coefficients. The model also offers explanations for why the green glasses form boomerang-shaped trends on many two-element variation diagrams and why certain compositions (Groups A and D) are more abundant than glasses with other compositions.

INTRODUCTION

APOLLO 15 GREEN-GLASS PARTICLES occur as ash-sized (mostly <100 μm) mafic spheroids in lunar soils and regolith breccias. Their primitive compositions and pyroclastic origin suggest that these particles probably derived from the lunar mantle without substantial interaction with the overlying crust. The glasses have thus been regarded as a reliable indicator of the Moon's interior composition (SPUDIS and RYDER, 1985). Also, the green-glass composition and the inferred source compositions have been used in models that describe large-scale lunar evolution (e.g., HUGHES et al., 1988; JONES and DELANO, 1989). Such use of green-glass based compositions suffers from our lack of understanding of the petrogenesis of green glass, and attempts to model its compositional characteristics have had limited success.

Understanding the origin of green glass depends on modelling compositional trends. These trends are difficult to determine because the individual particles are so small (~10–100 μm), and their compositional range is narrow. Thus, previous investigators have focussed on specific aspects only, such as major-element compositions (e.g., DELANO, 1979; RYDER, 1986), trace-element compositions (MA et al., 1981; GALBREATH et al., 1989, 1990), or petrographic occurrence (MCKAY et al., 1974; HEIKEN et al., 1974). No single study has combined all of these approaches with high enough precision to yield a comprehensive data base for individual particles on which detailed petrogenetic modelling can be based. In this paper, we establish such a data base, report and evaluate relationships between major- and trace-element compositions, and propose a new petrogenetic model for the formation of green glass. In a separate paper (STEELE, 1992), relationships between composition and petrographic features of individual green-glass beads are interpreted.

Early geochemical investigations concluded that no statistically significant variations in major-element concentrations exist among Apollo 15 green-glass beads (e.g., CAVARRETTA et al., 1972; CAMERON et al., 1972; WARNER et al., 1972; GLASS, 1972; CARUSI et al., 1972; RIDLEY et al., 1973; HLAVA et al., 1973). However, subsequent work by STOLPER et al. (1974) and WOOD and RYDER (1977) suggested that this was not the case. DELANO (1979) was the first to demonstrate that green-glass particles do not constitute a single, compositionally homogeneous group. In that study, precise electron microprobe (EMP) analysis of 416 particles revealed two closely spaced compositional clusters (designated Groups A and D) and some rarer, higher-Mg# particles (Groups B, C, and E) situated adjacent to these clusters (Mg# = mole fraction Mg/[Mg + Fe]). DELANO (1979) postulated that the groups represent five separate green-glass melts that were derived independently by partial melting of five different source regions. Using data from DELANO (1979), GROVE (1981) concluded that the trend of the green glasses required an Fe-rich phase in the residuum and postulated that the Group B compositional variation was caused by sulfide melt immiscibility.

MA et al. (1981) analyzed fifty-five vitric particles by instrumental neutron activation analysis (INAA), hoping to clarify green-glass petrogenetic processes by comparing the behavior of incompatible and compatible minor and trace elements. On two-element diagrams, their data plot as linear arrays, rather than clusters characterized by little internal systematic variation as DELANO (1979) had found for major elements. MA et al. (1981) classified their particles into three main groups, two of which formed roughly parallel trends. The largest (Group Alpha) was further subdivided into five smaller linear groups positioned roughly orthogonal to the direction of principal variation (e.g., MA et al., 1981; Figs.

TABLE 1. Major- and normalized trace-element concentrations in green-glass particles from splits of sample 15426. Oxide values in % (mass); trace element concentrations in μg/g (ppm).

Split	,9012	,154	,9012	,154	,9012	,154	,9012	,9012	,9012	,9012	,9012	,9012	,9012	,154	,154	,9012	,9012	,9012	
Group*	C	C	C	C	C	hB	hB	hB	hB	hB	hB	hB	hB	hB	hB	hB	lB	lB	
Sample	469	195	413	336	472	158	404	358	394	269	224	430	271	153	335	409	461	403	±
EMP:																			s_m**
SiO_2	48.26	48.24	48.15	48.07	47.88	46.83	46.49	46.29	46.24	46.21	46.28	46.00	45.77	46.24	45.71	45.81	47.29	47.32	0.2%
TiO_2	0.24	0.25	0.25	0.28	0.28	0.39	0.40	0.38	0.40	0.38	0.41	0.40	0.40	0.41	0.38	0.41	0.33	0.34	3%
Al_2O_3	7.88	7.89	7.92	8.07	7.94	8.15	8.13	8.10	8.15	8.20	8.10	8.07	8.19	8.07	8.16	8.08	8.07	7.98	0.4%
Cr_2O_3	0.575	0.586	0.552	0.564	0.538	0.539	0.534	0.496	0.513	0.518	0.537	0.554	0.503	0.571	0.527	0.516	0.537	0.549	2.5%
FeO	16.09	16.09	16.28	16.35	16.65	17.90	18.12	18.52	18.61	18.63	18.75	18.77	18.78	18.78	18.97	18.99	16.93	17.01	0.4%
MgO	18.19	18.00	18.11	17.66	17.80	17.19	17.20	17.08	17.04	17.03	16.98	17.24	17.12	16.82	17.24	17.08	17.96	18.04	0.3%
CaO	8.59	8.68	8.57	8.81	8.71	8.80	8.87	8.88	8.76	8.80	8.72	8.75	8.91	8.83	8.81	8.86	8.60	8.56	0.4%
MnO	0.25	0.25	0.22	0.25	0.24	0.27	0.26	0.25	0.28	0.23	0.26	0.26	0.32	0.27	0.28	0.27	0.28	0.25	5%
"Total"	100	100	100	100	100	100	100	100	100	100	100	100	100	100	100	100	100	100	
N	4	4	3	3	3	5	4	4	4	4	4	4	4	4	3	4	4	4	
INAA:																			$s^{\#}$
Na_2O	0.125	0.124	0.117	0.121	0.129	0.152	0.152	0.147	0.144	0.144	0.173	0.152	0.146	0.149	0.149	0.151	0.137	0.135	1.0%
Sc	36.2	36.3	34.4	35.9	36.1	36.0	35.8	36.0	36.0	36.1	36.1	36.9	36.5	36.2	36.5	36.5	35.2	36.2	1%
Cr_2O_3	0.556	0.558	0.550	0.554	0.551	0.538	0.532	0.532	0.533	0.534	0.533	0.553	0.539	0.538	0.540	0.539	0.546	0.552	1%
Co	53.0	54.2	59.4	56.4	58.6	67.0	68.6	71.0	72.1	72.6	73.8	71.7	72.2	72.6	73.3	73.3	63.1	61.9	0.5-1.5%
Ni	95	73	146	109	166	149	138	160	160	171	167	140	146	166	170	163	141	113	10-40%
La	0.656	0.682	0.664	0.782	0.820	1.554	1.582	1.548	1.584	1.531	1.708	1.400	1.458	1.508	1.548	1.509	1.073	1.003	3-8%
Sm	0.429	0.444	0.425	0.501	0.535	0.917	0.899	0.855	0.893	0.892	0.942	0.851	0.888	0.888	0.900	0.871	0.660	0.671	1%
Eu	0.161	0.135	0.161	0.151	0.188	0.267	0.289	0.285	0.282	0.282	0.224	0.263	0.254	0.231	0.290	0.302	<0.38	0.214	8%
Tb	0.121	0.113	0.120	0.136	0.146	0.215	0.199	0.190	0.226	0.226	0.252	0.217	0.245	0.208	0.236	0.234	0.188	0.177	8%
Yb	0.777	0.826	0.770	0.784	0.840	1.118	1.158	1.064	1.085	1.058	1.120	1.080	1.125	1.067	1.059	1.091	0.970	0.955	8%
Lu	0.141	0.122	0.111	0.125	0.124	0.153	0.172	0.173	0.163	0.169	0.166	0.141	0.159	0.170	0.173	0.172	0.159	0.148	6%
mass (μg)	36	76	114	61	43	47	82	99	124	70	36	71	90	94	43	106	49	174	

Split	,154	,9012	,9012	,9012	,9012	,9012	,9012	,154	,154	,154	,154	,154	,9012	,154	,9012	,154	,9012	
Group*	lB	lB	lB	lB	lB	hA	hA	hA	hA	hA	hA	hA	hA	lA	lA	lA	lA	
Sample	122	283	386	449	368	255	471	169	120	133	290	298	223	308	354	317	410	±
EMP:																		s_m**
SiO_2	47.64	47.21	47.09	46.89	46.95	45.95	45.67	45.70	45.64	45.79	45.38	45.63	45.40	45.67	45.66	45.57	45.30	0.2%
TiO_2	0.34	0.35	0.35	0.35	0.38	0.37	0.40	0.40	0.38	0.38	0.38	0.41	0.41	0.39	0.39	0.41	0.40	3%
Al_2O_3	8.06	8.02	8.15	8.19	8.10	7.91	7.89	8.07	8.10	7.72	8.11	7.92	7.99	7.97	7.82	7.84	7.97	0.4%
Cr_2O_3	0.518	0.522	0.539	0.558	0.525	0.557	0.564	0.539	0.552	0.568	0.568	0.531	0.532	0.541	0.560	0.559	0.581	2.5%
FeO	17.03	17.24	17.25	17.43	17.51	19.34	19.39	19.47	19.58	19.59	19.61	19.68	19.69	19.59	19.68	19.73	19.74	0.4%
MgO	17.53	17.88	17.73	17.61	17.59	16.85	17.07	16.90	16.86	16.91	16.96	16.96	17.03	16.89	17.09	17.04	17.10	0.3%
CaO	8.65	8.52	8.68	8.78	8.75	8.80	8.78	8.69	8.68	8.67	8.76	8.66	8.69	8.73	8.60	8.64	8.68	0.4%
MnO	0.24	0.31	0.27	0.25	0.19	0.248	0.259	0.248	0.251	0.278	0.308	0.240	0.327	0.264	0.260	0.258	0.271	5%
"Total"	100	100	100	100	100	100	100	100	100	100	100	100	100	100	100	100	100	
N	4	4	4	4	4	4	3	3	4	4	4	4	4	4	4	4	4	
INAA:																		$s^{\#}$
Na_2O	0.143	0.140	0.141	0.147	0.138	0.137	0.143	0.124	0.124	0.124	0.126	0.123	0.129	0.134	0.129	0.144	0.135	1%
Sc	35.9	36.3	36.3	36.2	35.6	36.7	36.4	36.5	36.9	36.6	36.6	36.7	36.7	37.1	37.1	36.8	37.3	1%
Cr_2O_3	0.540	0.548	0.548	0.543	0.534	0.542	0.541	0.537	0.542	0.538	0.536	0.541	0.544	0.544	0.544	0.553	0.550	1%
Co	63.6	62.8	63.9	64.7	66.2	75.9	76.0	75.7	75.5	76.2	75.9	75.9	75.7	75.6	77.1	79.0	76.4	0.5-1.5%
Ni	<413	108	127	140	<135	150	178	147	188	153	158	187	145	176	161	204	186	10-40%
La	1.231	1.123	1.166	1.220	1.232	1.259	1.269	1.116	1.169	1.138	1.204	1.185	1.075	1.056	0.825	1.024	1.021	3-8%
Sm	0.718	0.699	0.735	0.750	0.757	0.735	0.765	0.728	0.732	0.723	0.755	0.708	0.739	0.669	0.578	0.678	0.672	1%
Eu	—	0.227	0.200	0.232	0.369	0.221	0.212	0.227	0.220	0.284	0.256	0.184	0.274	0.236	0.236	0.234	0.207	8%
Tb	—	0.186	0.193	0.212	0.165	0.188	0.212	0.186	0.200	0.188	0.202	0.175	0.202	0.189	0.195	—	0.180	8%
Yb	0.921	0.936	0.971	0.943	0.999	0.957	0.990	0.953	0.830	1.032	0.986	0.990	0.934	0.915	0.864	0.917	1.051	8%
Lu	0.117	0.158	0.148	0.141	0.127	0.143	0.145	0.152	0.128	0.121	0.147	0.144	0.150	0.141	0.137	0.161	0.153	6%
mass (μg)	72	93	125	60	77	94	44	107	219	146	81	97	45	70	98	60	390	

3b, 4b). These investigators proposed that the green glasses had derived by various degrees of partial melting of heterogeneous source materials that formed a compositional continuum.

More recently, GALBREATH et al. (1989; 1990) combined EMP and secondary ion mass spectrometry (SIMS) techniques to analyze seventy green-glass particles. They used the classification scheme established by DELANO (1979), but rather than hypothesizing five discrete source regions for the groups A–E, they suggested instead that the groups could have been generated from three source regions that had experienced limited mixing.

Both the group designations and the petrogenetic model of MA et al. (1981) differed from those of DELANO (1979),

TABLE 1. cont'd.

Split	,154	,154	,154	,154	,154	,9012	,9012	,9012	,9012	,9012	,154	,154	,154	,9012	,9012	,9012	,154	
Group*	lA	lA	lA	lA	D	D	D	D	D	D	D	D	D	D	D	D	E	
Sample	172	139	198	303	327	390	267	282	423	470	332	326	161	374	439	460	137	±
EMP:																		s_m**
SiO_2	45.48	45.46	45.27	45.27	45.19	45.40	45.29	45.17	45.15	45.10	45.15	45.07	45.06	45.18	45.12	44.88	45.38	0.2%
TiO_2	0.39	0.36	0.40	0.41	0.45	0.41	0.41	0.41	0.44	0.42	0.40	0.44	0.42	0.43	0.41	0.42	0.45	3%
Al_2O_3	7.72	7.79	7.83	7.74	7.87	7.83	7.59	7.75	7.40	7.68	7.64	7.67	7.45	7.52	7.56	7.46	7.76	0.4%
Cr_2O_3	0.539	0.555	0.548	0.556	0.549	0.524	0.543	0.544	0.506	0.551	0.536	0.526	0.534	0.542	0.550	0.540	0.511	2.5%
FeO	19.79	19.89	19.90	19.93	19.56	19.77	20.01	20.02	20.09	20.09	20.15	20.16	20.28	20.28	20.31	20.47	19.38	0.4%
MgO	17.13	17.15	17.23	17.22	17.90	17.40	17.50	17.58	17.90	17.60	17.39	17.53	17.71	17.42	17.48	17.67	18.12	0.3%
CaO	8.72	8.59	8.57	8.66	8.31	8.46	8.45	8.36	8.30	8.36	8.51	8.42	8.32	8.39	8.37	8.33	8.17	0.4%
MnO	0.293	0.264	0.299	0.252	0.243	0.265	0.259	0.244	0.280	0.262	0.252	0.264	0.248	0.274	0.259	0.251	0.251	5%
"Total"	100	100	100	100	100	100	100	100	100	100	100	100	100	100	100	100	100	
N	4	5	4	4	5	4	4	4	4	4	4	4	4	4	4	4	4	
INAA:																		s#
Na_2O	0.131	0.121	0.138	0.132	0.147	0.122	0.125	0.140	0.126	0.138	0.125	0.170	0.134	0.149	0.142	0.136	0.147	1.0%
Sc	37.2	37.0	37.5	37.2	34.7	35.3	34.8	36.3	34.6	35.5	35.9	35.6	35.0	35.1	34.9	35.6	33.1	1%
Cr_2O_3	0.550	0.544	0.554	0.550	0.536	0.537	0.532	0.546	0.531	0.536	0.534	0.540	0.533	0.545	0.526	0.537	0.523	1%
Co	77.5	77.9	78.5	77.7	76.9	76.6	77.9	77.5	78.0	78.6	79.0	79.8	80.5	81.5	81.0	80.6	72.9	0.5-1.5%
Ni	169	144	171	159	146	152	169	181	142	158	156	189	145	184	171	173	131	10-40%
La	0.808	0.831	0.897	0.884	1.274	0.982	1.126	1.155	1.365	1.210	1.175	1.349	1.106	1.168	0.938	1.125	1.696	3-8%
Sm	0.568	0.587	0.583	0.595	0.799	0.659	0.686	0.721	0.781	0.740	0.754	0.860	0.705	0.725	0.674	0.740	0.970	1%
Eu	0.212	0.190	0.232	0.216	0.308	0.253	0.260	0.303	0.309	0.285	0.256	0.303	0.296	----	0.263	0.286	0.312	8%
Tb	0.154	0.174	0.181	0.186	0.235	0.169	0.166	0.215	0.204	0.182	0.212	0.206	0.188	0.236	0.184	0.227	0.234	8%
Yb	0.914	0.812	1.048	0.904	1.007	0.885	0.818	0.918	0.975	0.977	0.998	1.046	0.912	0.963	0.900	0.922	1.033	8%
Lu	0.133	0.143	0.155	0.146	0.218	0.137	0.120	0.147	0.151	0.145	0.135	0.150	0.127	0.137	0.137	0.139	0.152	6%
mass (μg)	101	121	104	68	72	184	115	51	92	47	37	55	114	54	65	58	89	

* Modified from classification of Delano (1979); see text.

** Uncertainties (±) presented for major elements determined by EMP analysis are typical values for the standard deviation of the mean (s_m, relative, in percent of concentration value) based on N replicate analyses of each bead. The high precision (low s_m) for some elements (e.g., SiO_2) results in part from normalization of the sums to 100% (see text for discussion).

\# Uncertainties (±) presented for elements determined by INAA are *random* uncertainties associated with counting statistics. The total uncertainty includes, in addition to this component, an average of 0.4% correlated component for normalized data (as in this Table) or an average of 5.5% correlated component for unnormalized data (as on some variation diagrams; see text for discussion).

---- No value obtained and no upper limit estimate made.

and some conclusions drawn by GALBREATH et al. (1990) differed from those of both earlier studies. From those works, the correspondence between the behavior of major and trace elements in Apollo 15 green glass, which is crucial to accurate petrogenetic modelling, cannot be uniquely determined. The present investigation was designed to provide a coherent set of major- and trace-element data and to identify compositional relationships that would provide clues and constraints to the petrogenesis and source of green glass. Particular effort was given to the acquisition of the most precise compositional data possible because compositional differences among green-glass particles are small. The major-element characteristics first observed by DELANO (1979) have been confirmed subsequently in other investigations (e.g., RYDER, 1986). Trace-element data have been presented in two studies to date (MA et al., 1981; GALBREATH et al., 1990), but cumulatively for a much smaller number of beads than analyzed in the major-element studies and with different compositional distributions shown in each data set (as discussed). Therefore, the present study places greater emphasis on obtaining precise INAA data for a large number of individual spherules, with subsequent EMP analysis of a subset of beads that exhibited the full range of trace-element compositions. This procedure enabled correlation of trace-element compositions with the better-known major-element compositions.

ANALYTICAL METHODS

Several analytical challenges had to be overcome to do a precise compositional survey of green glass. Individual beads are orders of magnitude lower in mass (tens to hundreds of micrograms) than samples we usually analyze by INAA (1–300 mg). We found that using a standard microbalance (Sartorius brand, Model 2405), we were unable to obtain the necessary weighing accuracy of < 1% (to be discussed). In addition, many important trace elements are present in relatively low concentrations in green glass (e.g., REE concentrations are only 2–5 times those of chondrites; MA et al., 1981; GALBREATH et al., 1990) and, for a bulk technique like INAA, this compounds the problem of low sample mass. Because of these combined difficulties, pertinent aspects of our analytical methods and assessment of their uncertainties are described in detail below.

Instrumental Neutron Activation Analysis

Green-glass beads were taken from two allocations (NASA subsplits ,9012 and ,154) of polymict regolith breccia 15426 (RYDER, 1985). Material was first examined under a binocular microscope while dry so that general characteristics of the bulk regolith could be described (e.g., variations in color, extent of consolidation). Addition of a few milliliters of ultrapure freon helped to remove most of the fine debris that was clinging to the green-glass particles and also provided a lower refractive index contrast between the beads and their surrounding medium, reducing surface reflectivity and thus allowing easier examination of morphology and internal features. The liquid also reduced the risk of sample loss by eliminating electrostatic forces. Freon was used because it was unlikely either to contaminate the samples

or to disturb their compositions (e.g., by leaching relatively mobile elements such as Na).

In order to maximize the precision of (INAA) data, only those particles greater than about 40 μg were chosen for analysis (selection rationale is further described by STEELE, 1992). Using a small nylon artist's brush, beads were transferred from the soil sample to a low-powered sonifying bath. Sonification (under freon) for 1–3 min removed adhering regolith from cracks and pits in the glass surfaces, as determined by inspection using a binocular microscope.

365 beads were chosen for analysis (223 from split 15426,9012 and 142 from 15426,154). These beads total about 50 mg in mass and included all of the >40-μg particles present in these two allocated splits, which collectively constituted ~2 g of the 15426 parent sample. The beads from each allocation were sealed into a separate, evacuated ampoule of ultrapure silica (Suprasil T21, Heraeus Amersil) for neutron activation. Chips of an in-house synthetic glass were used as elemental standards, and these were sealed into a third silica ampoule. The ampoules were irradiated for 144 h in a thermal neutron flux of 4.5×10^{14} $cm^{-2}s^{-1}$ in the flux trap of the University of Missouri Research Reactor (MURR; Columbia, MO). Each bead was then weighed and placed in an individual ampoule for radioassay. Initial radioassays were done between one and six days after the end of irradiation. Precise concentration values for several elements (Sc, Cr, Co, FeO, Sm, and Na) were obtained in counting times as short as 20 min, depending on the sample mass. By this procedure, particles of unusual composition were identified quickly and reassayed for longer times, if necessary, to improve counting statistics. A subset of beads was radioassayed again between six and fourteen days after irradiation to improve precision for the longer-lived isotopes. Data were reduced using techniques partially described by LINDSTROM and KOROTEV (1982). Other analytical details are given by KOROTEV (1991).

Electron Microprobe Analysis

After INAA and petrographic examinations of individual particles were completed, each of fifty-two of the 365 green glasses was mounted in a drop of epoxy on the end of a brass cylinder (radius 0.125 inches; height 0.25 inches). After the epoxy had cured, each mount was hand ground to a 1-μm finish, exposing a significant diameter of each bead (hundreds of μm). Samples were analyzed with a JEOL 733 electron microprobe using standard wavelength-dispersive techniques. Operating conditions were 15 keV and 20 nA beam current, with a 20-μm beam diameter used both for standards and unknown samples. The oxides determined included SiO_2, TiO_2, Al_2O_3, Cr_2O_3, FeO, MgO, CaO, and MnO; and counting times varied from 10–40 sec, depending on the oxide concentration in the unknowns. All data were reduced using the correction procedures of BENCE and ALBEE (1968). Natural and synthetic mineral and glass standards (JAROSEWICH et al., 1979) were used for calibration and monitoring of accuracy and precision during data acquisition. In addition, either of two green-glass beads was used as a "working standard" during all analytical sessions. A working standard was reanalyzed after every three unknown samples (about every twelve analyses).

Precision and Accuracy

Assessment

Accurate characterization of compositional differences and trends is strongly dependent on analytical precision; substantial random analytical uncertainties and correlated analytical errors have obscured the characterization of the green-glass beads by some previous investigators (to be shown). Therefore, we anticipated that thorough understanding of analytical precision and accuracy for both INAA and EMP data would be essential. Two types of uncertainties affect individual green-glass particles that have been analyzed by INAA: random and correlated. Random uncertainties arise mainly from counting statistics during INAA and, for elements determined most precisely by this technique, are estimated to be from 0.5–1.5% (one standard deviation relative), depending on the element. Correlated uncertainties derive from several sources and involve systematic variations of parameters that equally affect the determination of all elements in a single sample. Neutron flux gradients during irradiation, slight irreproduceability of counting geometry, and other factors inherent in INAA are estimated to contribute approximately 1.5% (relative) correlated uncertainty to the determination of element concentrations. The largest source of correlated uncertainty arises from determination of bead masses. We found that, in the mass range in question (median mass: 89 μg), the microbalance cannot yield mass determinations that are sufficiently reproducible for use in the calculation of precise absolute element concentrations. Although rep-

TABLE 2. Average compositions of Apollo 15 green glass groups, from data of Table 1. Oxide concentrations in percent, trace element concentrations in μg/g.

Group: (N)	C (5)		hB (11)		lB (7)		hA (8)		lA (8)		D (12)	
	mean	±95%	mean	±95%	mean	±95%	mean	±95%	mean	±95%	mean	±95%
SiO_2	48.12	0.19	46.17	0.22	47.20	0.21	45.64	0.17	45.46	0.14	45.15	0.08
TiO_2	0.259	0.023	0.397	0.008	0.349	0.015	0.391	0.013	0.394	0.013	0.422	0.010
Al_2O_3	7.94	0.09	8.13	0.03	8.08	0.07	7.96	0.11	7.83	0.08	7.62	0.09
Cr_2O_3	0.554	0.004	0.537	0.004	0.545	0.006	0.540	0.002	0.549	0.003	0.536	0.004
FeO	16.29	0.29	18.62	0.23	17.20	0.20	19.54	0.11	19.78	0.010	20.10	0.16
MgO	17.95	0.27	17.09	0.08	17.76	0.18	16.94	0.07	17.11	0.09	17.59	0.11
CaO	8.67	0.12	8.82	0.04	8.65	0.09	8.72	0.05	8.65	0.05	8.38	0.04
MnO	0.244	0.016	0.267	0.015	0.256	0.035	0.270	0.027	0.270	0.014	0.258	0.007
Na_2O	0.123	0.006	0.15	0.005	0.140	0.004	0.129	0.006	0.133	0.006	0.138	0.009
Sc	35.8	1.0	36.2	0.2	36.0	0.4	36.6	0.1	37.1	0.2	35.3	0.3
Co	56.3	3.4	71.7	1.4	63.7	1.3	75.8	0.2	77.5	0.9	79.0	1.1
Ni	118	47	158	8	126	19	164	15	172	15	164	10
La	0.72	0.09	1.54	0.05	1.15	0.08	1.18	0.06	0.92	0.08	1.16	0.08
Sm	0.47	0.06	0.891	0.017	0.71	0.04	0.736	0.015	0.62	0.04	0.74	0.04
Eu	0.159	0.024	0.270	0.017	0.218*	0.023	0.235	0.028	0.220	0.014	0.284	0.015
Tb	0.127	0.017	0.222	0.013	0.187	0.017	0.194	0.010	0.180	0.012	0.202	0.015
Yb	0.80	0.04	1.093	0.022	0.96	0.03	0.96	0.05	0.93	0.07	0.94	0.04
Lu	0.125	0.013	0.165	0.007	0.142	0.014	0.141	0.009	0.146	0.008	0.145	0.016

* excludes one value.

licate weighing of a set of test particles during a single sitting at the microbalance yielded deviations commonly on the order of only ±1 μg (i.e., ~1% on average), reweighing of the same particles during later sessions (e.g., days or weeks later) yielded both random and systematic differences in mass determinations when compared to the original values. We therefore recognized that weighing error was significant in our INAA determinations since replicate weighings of the 365 analyzed particles required several days. The percentage of change between original and subsequent weighings of the test particles was found to average ~4% relative. This value serves as a rough estimate of the magnitude of the correlated uncertainty from weighing for this study. Thus, the total correlated uncertainty affecting individual green glasses is estimated to be 5.5% on average. As will be shown, this uncertainty, if uncorrected, is sufficient to distort substantially the interpretation of INAA data.

Three to five (average of four) EMP analyses were done on each of fifty-two particles that had been analyzed by INAA. Only those EMP analyses that totalled between 98.5 and 101.5 wt% were accepted. These were first normalized to 100 wt% and then averaged to yield the values in Table 1 (group averages are also presented; see Table 2). The uncertainty associated with these averages is expressed as the standard deviation of the mean value (s_m) for four analyses. The s_m values express random uncertainty for these averages. They are the only uncertainties expressed when major elements are compared with each other. We note that the uncertainties for the major elements reported in Table 1 reflect the observed reproducibilities of the normalized analyses (s_m) but not estimates of absolute error such as might arise from the normalization process, heterogeneity in the standards, or errors in the Bence-Albee interference correction routine.

For those beads analyzed by EMP, correlated uncertainties in the INAA data were decreased significantly by elimination of weighing error. We did this by multiplying concentrations obtained from INAA by the ratio FeO_{EMP}/FeO_{INAA}. Normalization of trace-element to major-element data is best done using Fe because Fe is determined with good relative precision by both techniques and good absolute precision by EMP. This procedure removes any correlated error inherited from weighing and from INAA (e.g., due to flux gradients) but it appends the uncertainty of the FeO_{EMP} values used in the normalization. However, this is a much smaller uncertainty (average FeO s_m ± 0.4%, vs. ±5.5% in the unnormalized data), so the approach used here (INAA followed by replicate EMP analyses plus normalization) minimizes uncertainties to the extent that these analyses of Apollo 15 green glass appear to be the most precise obtained to date.

Representation

Figures presented in this paper contain representations of analytical error that reflect the nature of the uncertainties discussed above. Diagrams showing major elements only bear the conventional one-s_m crosses (indicating one standard deviation of the mean value or appropriate arithmetic propagations thereof). Figures comparing INAA data show a small cross representing one-s_m random uncertainty (one sample standard deviation) superimposed on a large, diagonal, correlated-uncertainty bar. Normalized trace-element diagrams retain the same small one-s_m cross but show a short correlated uncertainty bar that denotes uncertainty in the determination of FeO by EMP rather than those imparted by INAA and weighing. Diagrams combining EMP- and INAA-determined quantities show one-s_m uncertainties for the major element, while uncertainty in the trace-element data incorporates both one-s_m random error (counting statistics) and one-s_m uncertainty in the FeO concentration to which the INAA data are normalized.

Assessment of uncertainty was restricted to internal precision in this study. Expressions of uncertainty do not include estimates of accuracy of the measurements for either analytical technique, and different analytical standards were used for INAA and EMP analyses.

COMPOSITIONAL DISTRIBUTION OF APOLLO 15 GREEN GLASS

Major- and Trace-element Studies: Past and Present

Variation diagrams showing INAA data obtained in this study illustrate both the compositional distribution of Apollo 15 green glass and the effects of correlated uncertainty. Weighing errors distort the data by generating linear trends (Fig. 1a) where little actual systematic compositional variation is present (Fig. 1b). However, even on plots that incorporate substantial correlated uncertainty, compositional clusters are visible. Some particles with low Sc concentrations (inverted triangles; Fig. 1) appear to occupy a discrete compositional field. One particle that appeared to belong to this group on the unnormalized plot (point E; Fig. 1a) actually has significantly lower Sc (Fig. 1b) and higher Sm (Fig. 2) concentrations and thus represents a distinct composition. The remaining beads appear to form a diffusely bounded cluster on the Sc-FeO plot, but an examination of other diagrams reveals that subdivisions occur within this suite. Compositional hiatuses separate samples symbolized by triangles from those symbolized by diamonds (Fig. 3), and both are different from samples symbolized by squares (Fig. 2).

Thus, we can classify the 365 particles analyzed in the present study as comprising six trace-element clusters. If the point labelled "E" (Figs. 1, 2) is a member of another cluster

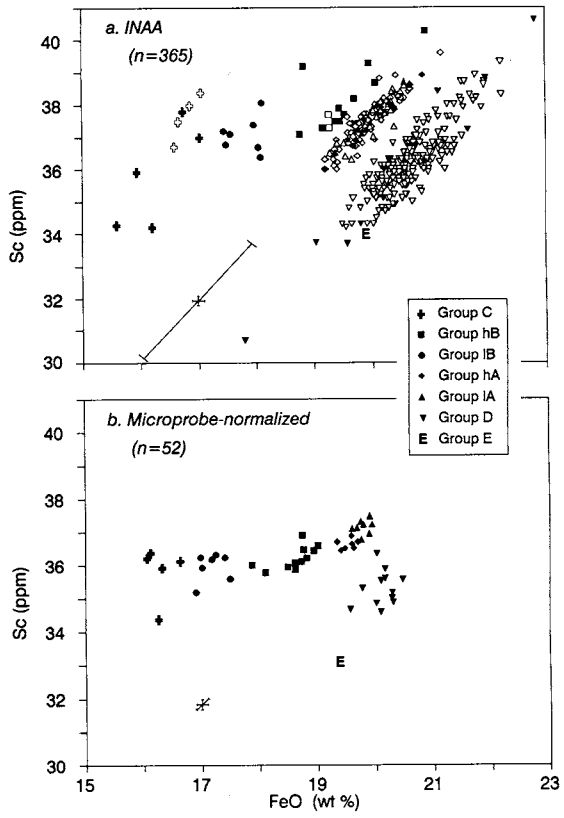

FIG. 1. Scandium (ppm) is shown plotted against FeO (wt%) for both INAA- and EMP-normalized data. Throughout this paper, beads that were analyzed by EMP are shown as filled symbols, while open symbols designate beads that received trace-element analyses only. On INAA diagrams (a), the filled symbols denote the prenormalization positions of the same beads that were subsequently normalized (b). The effect of normalization is to dramatically diminish the compositional scatter, revealing that the apparent extensive compositional trends encompass much more limited actual variation. Cross indicates one-s_m (random uncertainty); diagonal bar indicates correlated uncertainty. See text for a discussion of group names and uncertainty depiction.

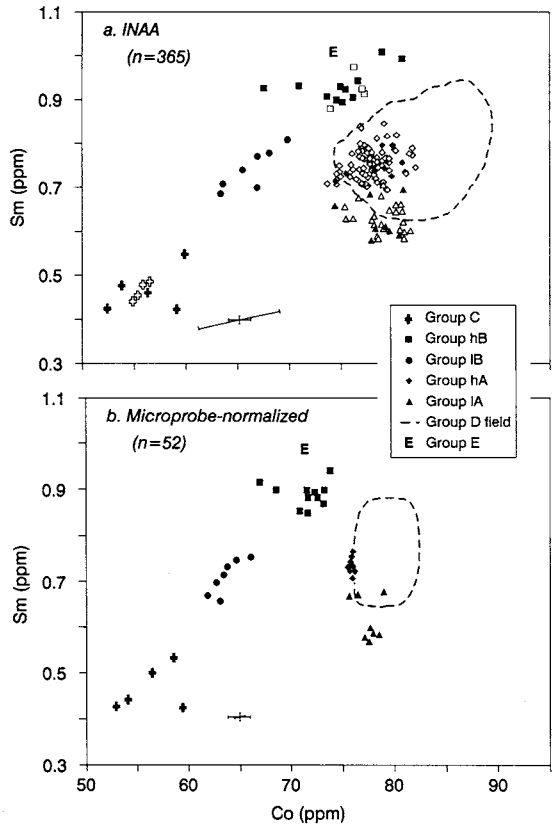

FIG. 2. Samarium (ppm) plotted against Co (ppm). As in Fig. 1, several compositional clusters appear, and reduction of correlated error is obvious on the normalized plot (b). Samarium was chosen because, of the REEs, it is determined with the best precision. Symbols as in Fig. 1.

rather than merely an outlier, the number of clusters becomes seven. In addition to being visually apparent on variation diagrams, these clusters are statistically distinct as indicated by results of the *F*-test (for similarity of variance) and the *t*-test (for comparison of means; e.g., DAVIS, 1986; examples in Table 3). We interpret this result to mean that these compositional clusters represent distinct groups, as has been done for green glass previously in the literature (although "group" as used in this paper refers only to the statistically significant clustering and does not necessarily carry petrogenetic connotations). Examination of the major-element data for fifty-two of these particles discloses the correspondence between these groups and those defined initially by DELANO (1979) (Fig. 4). This correspondence is straightforward, although some features revealed by trace elements are not visible in major-element data. Because the green-glass group names A–E (DELANO, 1979) are established in the literature, we use them in describing the groups in this paper. The Sc-FeO hiatus observed in the present study (Fig. 1) corresponds to the hiatus DELANO (1979) observed between Groups A and D. The large group to the high-FeO side of this break constitutes Group D. The single low-Sc particle appears to belong to Group E (interpretation supported by the data of GALBREATH et al., 1990). The particles immediately to the low-FeO side of the hiatus (Fig. 1) constitute Group A. Although an incompatible trace-element hiatus occurs within Group A (Fig. 2), a complementary major-element break is not visible in either the major-element data of DELANO (1979) or those of the present study (Fig. 4). The two Group-A subgroups (designated "hA" and "lA"; Fig. 3) do not overlap in either major- or trace-element abundances, but the major-element ranges abut and form a compositional continuum such that two groups could not be recognized using major elements alone (Fig. 5).

The low-FeO green glasses include members of both Groups B and C. Although these two groups appear continuous on some variation diagrams (e.g., Fig. 1), data of both DELANO (1979) and the present study indicate that Group C is not merely a continuation of the Group B trend. The resolution of these low-FeO particles into separate groups becomes especially apparent when MgO is plotted against incompatible trace elements (e.g., Fig. 5). Furthermore, on several variation diagrams showing unnormalized data, Group B shows a compositional break that divides its trend roughly in half (Figs. 2a, 3). On diagrams showing normalized data, the break is even better defined (Figs. 2b, 5). Statistical

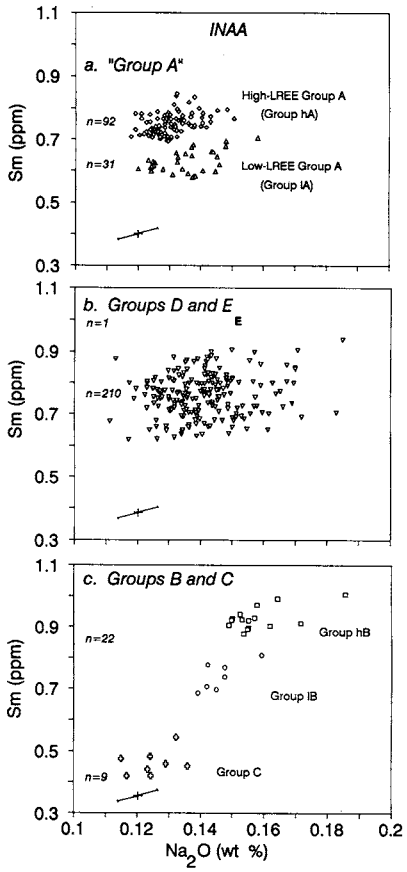

FIG. 3. Plot of Sm (ppm) vs. Na_2O (wt%), showing a breakdown of the groups evident on Figs. 1 and 2. (a) Group A, which appeared to be a single group on both previous figures, actually consists of two groups separated by a well-defined compositional hiatus. (b) As in Fig. 1, Group D occupies a larger compositional field. The single Group E particle displays higher Sm value but a Na_2O concentration which is indistinct from those of Group D. (c) The hB, lB, and C clusters align to form a positive linear array on this plot. Symbols as in Fig. 1.

TABLE 3. Comparison of mean values for some oxides and elements, Groups hA-lA and hB-lB.

	F stat (α=0.05)	s^2 differ?	t stat (α=0.10)	means differ?
hB *vs.* **lB:**				
Al_2O_3	2.46	no	1.72	yes
FeO	2.32	no	9.87	yes
MgO	2.53	no	8.81	yes
CaO	2.70	no	4.68	yes
Na_2O	3.86	no	3.24	yes
Sc	1.61	no	1.58	yes
Co	2.24	no	8.77	yes
Sm	2.11	no	11.91	yes
Lu	2.36	no	3.72	yes
hA *vs.* **lA:**				
Al_2O_3	2.00	no	2.23	yes
FeO	1.23	no	3.78	yes
MgO	1.77	no	3.46	yes
CaO	1.19	no	2.36	yes
Na_2O	1.2	no	1.27	no
Sc	2.71	no	5.52	yes
Co	25.41	yes	4.15	yes
Sm	6.97	yes	6.66	yes
Lu	1.31	no	0.96	no

F- and *t*-tests show that the divisions seen in both Groups A and B are significant (Table 3).

Many of the green-glass particles analyzed by EMP were chosen because they plotted at extremes in their respective groups on the INAA plots (Figs. 1a, 2a). Therefore, their normalized positions should approximate the trace-element boundaries of each group (Fig. 1b, 2b); from our data, the boundaries of these groups are distinct. This relatively precise definition of the groups, made possible by precise trace-element data, enables an evaluation of the group classifications made by previous investigators. Although DELANO (1979) defined five discrete compositional groups, their distinctiveness has been ambiguous. On major-element plots (e.g., DELANO, 1979, Fig. 2), Groups A, B, and C (likewise, D and E) could be interpreted as forming a compositional continuum, as might result from a single continuous process. In fact, GROVE (1981) implied a continuously sampled process in his petrogenetic model for Groups A and B. However,

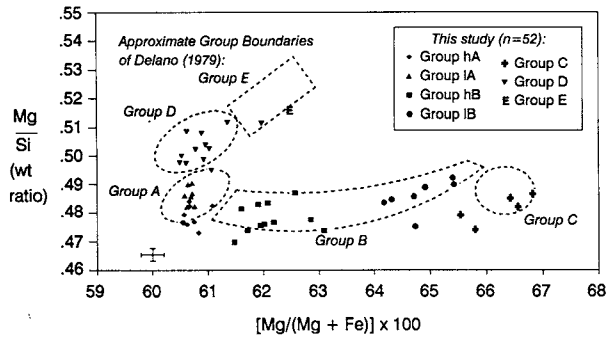

FIG. 4. Plot of Mg/Si (wt ratio) vs. Mg#. The major-element groups defined initially by DELANO (1979) and those evident in the trace-element data of the present study correspond consistently, although certain features, such as the divisions within Group A, are not resolvable in major-element data.

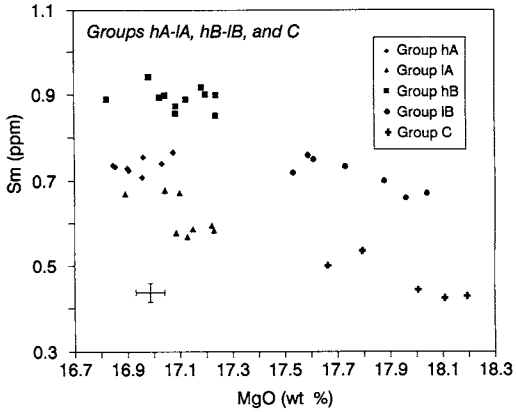

FIG. 5. Sm (ppm) plotted against MgO (wt%), illustrating the distinctiveness of Groups hB, lB, and C. On several plots (e.g., Figs. 1, 2), these three groups appear to form compositional continua, a feature that is not evident on this variation diagram.

trace-element data strongly indicate that the groups defined originally by DELANO (1979) are indeed discrete because the apparent continua seen in major-element data (A-B-C and D-E) are not maintained for all elements (e.g., Figs. 2, 3, 5).

We believe that another classification scheme (that of MA et al., 1981) is biased because the entire green-glass compositional spectrum was not well represented among the data used to define it and because the authors did not recognize correlated analytical uncertainty. The majority of the samples (93%) of MA et al. (1981) are of Group A composition (Fig. 6) and, as a result, these investigators did not have enough non-A glasses to distinguish Group D as a separate group. In addition, none of their particles was of Group C composition. Correlated uncertainty is evidently present in their data since

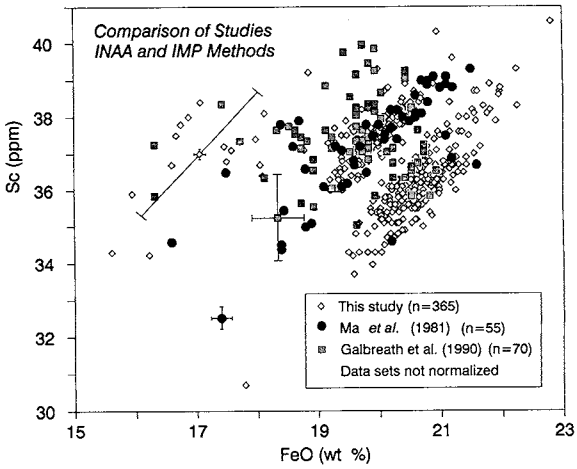

FIG. 6. A plot of Sc (ppm) vs. FeO (wt%) that compares the compositional distribution of green glasses analyzed in the present study and those found by MA et al. (1981) and GALBREATH et al. (1990). Most of the MA et al. (1981) beads were of Group A composition; only four belong to Group D. These investigators used a bulk technique (INAA) to analyze the minute particles, and their data appear, like ours, to contain correlated error. GALBREATH et al. (1990) used SIMS and EMP techniques to analyze particles in thin section. Their stated uncertainties do not appear to incorporate a correlated component, but they are relatively large (cf. Fig. 1b).

their particles form "trend" lines coincident with those seen in the present INAA study in which weighing error is known to be the predominant cause (Fig. 6). Because the classification of DELANO (1979) includes all observed compositions of Apollo 15 green glass and because it describes their division into discrete compositional groups, it is the more useful characterization of compositional groupings in Apollo 15 green glass, although our data show that refinement of "Group A" and "Group B" into two groups each is warranted (Figs. 2, 3, 5).

GALBREATH et al. (1990) used the classification of DELANO (1979) but, on the basis of incompatible trace element (ITE) vs. Co plots, cast groups A and D into a "low-Co" trend and Groups B and C into a "high-Co" trend, while Group E remained separate. While we concur that Groups hB and lB do form linear trends on variation diagrams that involve Co, our more precise trace-element data do not support an analogous linear trend for Groups A and D, either individually or when considered jointly (Fig. 2).

REE Patterns

The variation diagrams discussed above suggest that Apollo 15 green glass consists of clusters showing limited internal systematic variation, with the exception of Groups hB and lB, which align to form simple linear trends. REEs (especially LREEs) have proven particularly useful for distinguishing these groups. When REEs are examined, some divisions appear that are not revealed by other elements (e.g., that between hA and 1A; Fig. 3), and other divisions are enhanced (e.g., that between hB and both hA and 1A; Fig. 2). However, with the exception of Sm, random uncertainties affecting REE determinations are relatively large (Table 1). Correlated uncertainties in INAA data present additional complications because, although they do not affect the ratios among REEs in a single sample, they alter the apparent absolute concentrations. For these reasons, comparison of REE concentrations among individual green-glass particles using INAA data alone is difficult.

Once correlated uncertainty is reduced by normalization, the now precise REE concentrations for all particles in a single green-glass cluster can be averaged and resultant REE patterns compared. Figure 7 compares the chondrite-normalized REE abundances for the average composition of each of the green-glass groups. Most of these patterns show slight HREE enrichment, a finding consistent with that of MA et al. (1981) but inconsistent with that of GALBREATH et al. (1990). Although identical in average Yb and Lu values, Groups hA and 1A have significantly different LREE averages, a result previously evident (Fig. 3; Table 2). Group D is unique among all Apollo 15 green-glass groups in showing no significant Eu anomaly on average. The single Group E particle is clearly different from the Group D average in showing higher LREE concentrations and a negative Eu anomaly. Group C has the lowest REE concentrations of all the Apollo 15 green-glass groups, an observation consistent with findings of GALBREATH et al. (1990). Groups hB and lB differ significantly from each other in average concentrations of both LREEs and HREEs, and the change in REE slope with decreasing REE concentration is consistent with that observed in the other groups.

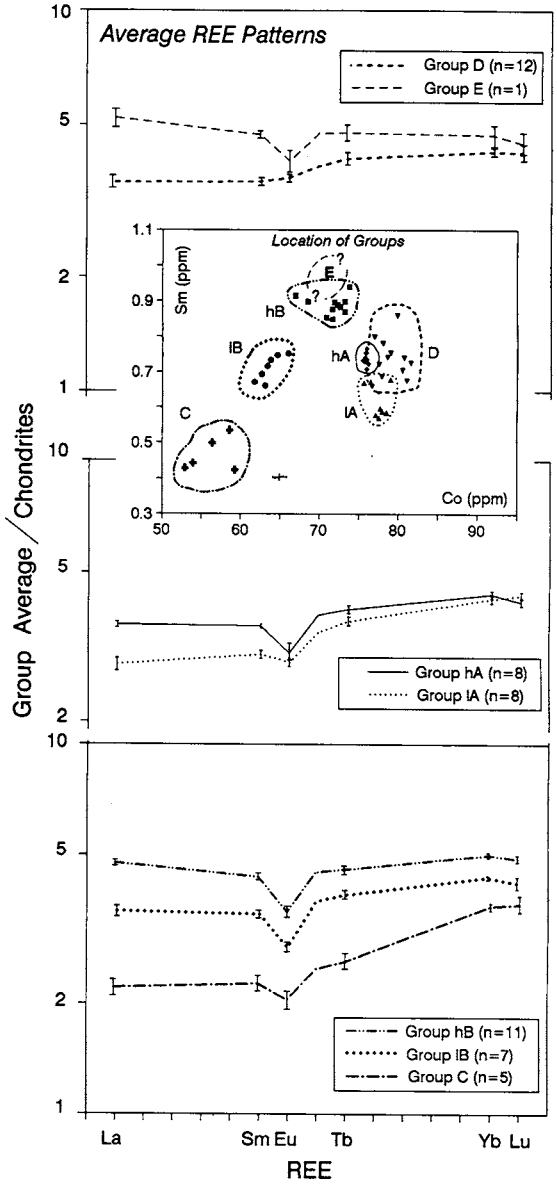

FIG. 7. Average REE concentrations normalized to nonvolatile Cl chondritic values (Cl abundances from ANDERS and EBIHARA, 1982, times 1.38) for all of the defined Apollo 15 green-glass groups. Uncertainty is expressed as S_m for n average FeO-normalized analyses for each group. This figure supports the autonomy of the green-glass groups because the average REE display statistically significant differences in pattern slope, extent of Eu depletion, and absolute abundances.

The hypothesis that compositional clustering is a fundamental characteristic of lunar volcanic glasses (e.g., DELANO and LIVI, 1981; DELANO, 1986) appears to be true for all Apollo 15 green-glass groups and is a general aspect of green-glass behavior that is more consistent than previously believed. The possibility remains of further subdivision too subtle to detect using the present set of elements and present level of analytical precision. Although these clusters suggest

that the glasses were formed by discrete events, they do not necessarily suggest that the clusters came from different compositional sources or that they formed by different petrogenetic processes, as we show below for the two Group B clusters.

PETROGENESIS OF APOLLO 15 GREEN GLASS

Each Apollo 15 green-glass compositional group shows some interelement correlation outside of analytical uncertainty. The trends are generally weak, owing to the narrow range of compositional variation within each group, but they still furnish information on the petrogenetic history of the particles. DELANO (1979) attributed the limited variation within Groups A, C, D, and E to either high-pressure fractional crystallization or varying percentages of partial melting in five separate source regions. MA et al. (1981) also suggested minor fractional crystallization, to explain intragroup variation within their Group Alpha (equivalent to Group A). Neither study cited specific phase compositions or proportions that would satisfy the observed variations within the green glass groups. GROVE (1981) suggested a model involving an immiscible sulfide melt. This model explains many of the major element trends but does not address trace element variations. The data obtained in the present study have clarified ambiguities in green-glass compositional trends, and we use them below to assess petrogenetic hypotheses.

Constraints from Pearce Element Ratios

Mineralogical information relevant to green-glass particles is largely absent, so some previous investigators (e.g., GALBREATH et al., 1990) have used Pearce diagrams to decipher causes of compositional variation. Pearce element-ratio diagrams (PEARCE, 1978, 1987; STANLEY and RUSSELL, 1989a,b,c; NICHOLLS, 1988; RUSSELL et al., 1990), also known as molecular proportion ratio (MPR) diagrams (ROLLINSON and ROBERTS, 1986), are discriminatory diagrams that were developed for the following three purposes (STANLEY and RUSSELL, 1989a): to determine whether rocks are cogenetic, to identify the principal minerals involved in differentiation, and to evaluate the extent to which those minerals were involved. An incidental effect is compensation for the problems that closure creates in the examination of major-element data (PEARCE, 1987). The diagrams have an additional advantage in that they are not limited to assessment of simple fractional crystallization but can disclose a wide range of material transfer processes, providing that at least one extensive variable (e.g., mass or number of moles of a particular element) is conserved in the system of interest (STANLEY and RUSSELL, 1989b).

Green-glass liquidus phases were likely restricted to ferromagnesian minerals (GREEN and RINGWOOD, 1973), so DELANO (1979) used Al and Ca concentrations as Pearce-ratio denominators. His assessment suggested that olivine fractionation alone was not responsible for compositional variation in any of the groups, so orthopyroxene (the next most plausible liquidus phase; STOLPER et al., 1974) may have been involved. GALBREATH et al. (1989, 1990) used Zr to create diagrams that tested for typical basaltic minerals and suggested that, along with olivine and orthopyroxene, clinopyroxene and plagioclase were also among the possible controls of intragroup compositional variation in all groups. Below, we evaluate the applicability of Pearce diagrams to green glass.

The PEARCE.PLOT Turbo-Pascal programs (STANLEY and RUSSELL, 1989b,c) were used to construct Pearce diagrams using the data obtained in the present study. Figure 8 shows various denominators that produce regression lines (calculated using the average-error axis method; STANLEY and RUSSELL, 1989b) that have intercepts within 2σ of the origin for Group D; results are similar for all other groups

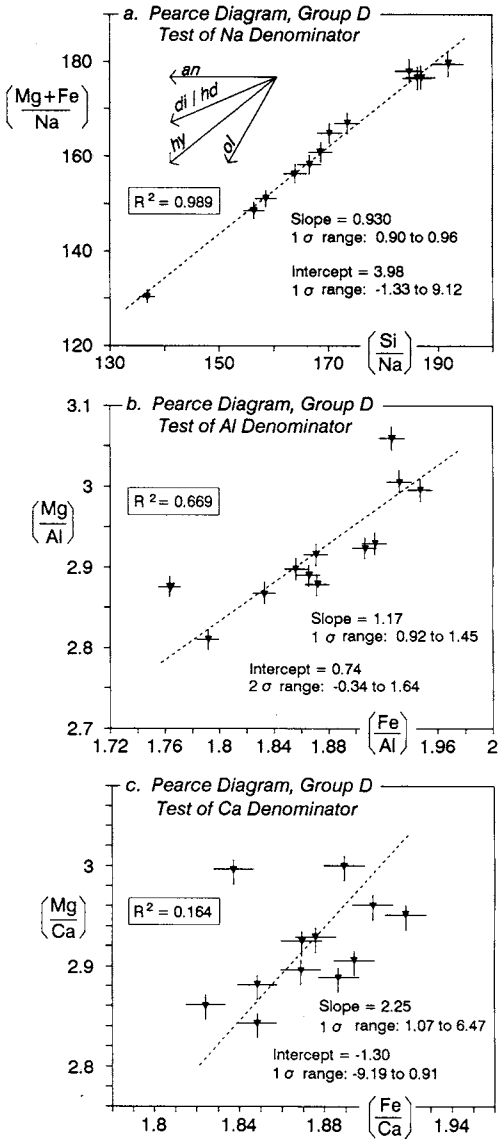

FIG. 8. Pearce element ratio diagrams for Group D. These plots, constructed with various denominators, all show intercepts within 2σ of the origin, indicating that the use of these diagrams in drawing petrogenetic conclusions would be invalid. Uncertainties are presented as ranges because, on plots of this type, confidence limits on both slope and intercept are asymmetric (STANLEY and RUSSELL, 1989b).

and other elements, including ITEs (not shown). A zero intercept implies that the quantity selected for the denominator of the ratio is unconserved (NICHOLLS, 1988; STANLEY and RUSSELL, 1989b). Thus, no constituent appears to have behaved in a "conserved" fashion in any Apollo 15 green-glass magma. This result indicates that the use of Pearce diagrams as petrogenetic indicators for Apollo 15 green glass is not valid (e.g., PEARCE, 1987). We also used PEARCE.PLOT to calculate uncertainties on the intercept of the regression lines presented by GALBREATH et al. (1990), as none were given in that study. In the majority of cases, these are within 1σ of the origin, negating the validity of the use of these diagrams as petrogenetic indicators, a predictable outcome, as the denominator these investigators chose (Zr) was effectively unconserved by virtue of its uncertainty alone ("<10%", GALBREATH et al., 1990, p. 2566; cf. range of data on their Fig. 5).

Mixing (or assimilation), inhomogeneity of the source region, or differentiation of a phase assemblage that affected every element in a system are all reasons why a suite of comagmatic samples might be characterized by having no conserved elements (RUSSELL and NICHOLLS, 1988). We investigate below which of these causes might pertain to Apollo 15 green glass.

Batch Equilibrium Melting: Groups hB and lB

Groups hB and lB collectively produce compositional trends that are also evident for Group lB alone on most variation diagrams. Two aspects of hB-lB trends are of particular interest because they are not typical of basaltic or picritic suites on Earth. Nickel and Co correlate positively with incompatible elements such as the REE, and SiO_2 correlates positively with Mg#. Previous workers have suggested various schemes to explain these trends, including source heterogeneity or mixing (e.g., DELANO, 1979; GALBREATH et al., 1990; SHEARER et al., 1990) and uncommon or poorly understood igneous processes (e.g., GROVE and LINDSLEY, 1978; GROVE, 1981; DELANO and LINDSLEY, 1982).

Because Ni^{2+} and Co^{2+} are compatible in olivine and pyroxene, whereas REE are incompatible, positive correlations among Ni, Co, and REE are not expected in mafic igneous suites that are related by simple igneous processes such as partial melting or crystal fractionation. However, recent investigations suggest that Ni becomes less compatible in olivine as f_{O_2} decreases (COLSON, 1990; EHLERS et al., 1991). In an extension of these studies, we find that, in compositions similar to Group hB-lB, Ni and Co become incompatible in olivine and low-Ca pyroxene at f_{O_2} values 2–4 log units below the iron-wüstite buffer owing to partial reduction to the metallic state but continued solubility in the silicate liquid (STEELE et al., 1991). Incompatible behavior of Ni and Co at low oxygen fugacity preserves the possibility that the positive correlations among Ni, Co, and REE in Group hB-lB can be explained principally by a traditional equilibrium melting model with, at most, minor contributions from assimilation, source heterogeneity, sulfide immiscibility, or other mechanisms that have been proposed to explain these trends.

Using our experimentally determined partition coefficient (opx/melt) for Co at low f_{O_2} (equal to 0.35; STEELE et al., 1991, and our unpubl. data) and a Sm partition coefficient calculated from COLSON et al. (1988) as 0.0025, we have used a batch equilibrium melting model to predict the correlation between Sm and Co in Groups hB and lB (Fig. 9). The amount of melting is not estimated by this model but is chosen to be generally consistent with that proposed by other investigators (GREEN and RINGWOOD, 1973). Although the fit of the model to the trend of the data is excellent, some scatter in excess of analytical uncertainty remains. This scatter can be explained by the effects of minor secondary processes, such as assimilation of other material during ascent of the magma or minor source heterogeneity.

A batch equilibrium model can also explain the positive correlation between SiO_2 concentration and Mg# if pressure is sufficiently high, as originally suggested by GROVE and LINDSLEY (1978) and shown quantitatively by COLSON and STEELE (1991). At high pressures (e.g., 10 kbars), the olivine-orthopyroxene reaction curve (for example, in the An-Fo-SiO_2 ternary system) becomes a cotectic along which the concentration of SiO_2 decreases as temperature decreases, a trend more pronounced at pressures higher than 1 atm (See Fig. 10). If the source region is sufficiently pyroxene-rich for melting or crystallization to occur along this cotectic, both Mg# and SiO_2 concentration will decrease with decreasing temperature, potentially explaining the positive correlation between them.

We have used the phase-equilibria program SILMIN (GHIORSO et al., 1983) to model the compositions and proportions of phases on this cotectic at 10 kbars as a function of the degree of partial melting of a hypothetical green glass source composition (Fig. 11). We constructed the source composition by adding olivine and pyroxene to a typical Group B composition. These phases were added in the proportions and compositions predicted by SILMIN to be in equilibrium with Group B. Because the SILMIN calculations do not consider Al_2O_3 or CaO concentrations in olivine or low-Ca pyroxene, Al_2O_3 concentrations in these phases were

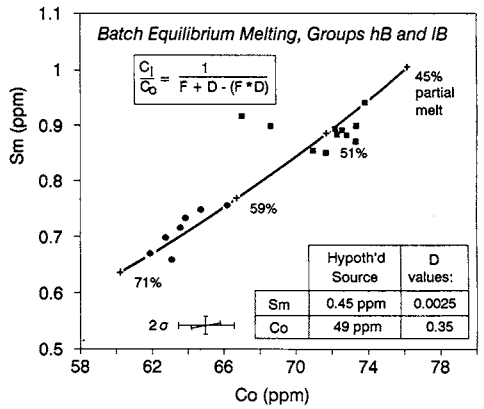

FIG. 9. The model for batch equilibrium melting, as applied to Groups hB and lB. If Co and Ni behave as mildly incompatible elements in the green-glass source region, then the positive correlation between these elements and REE can be explained to a first approximation by this model.

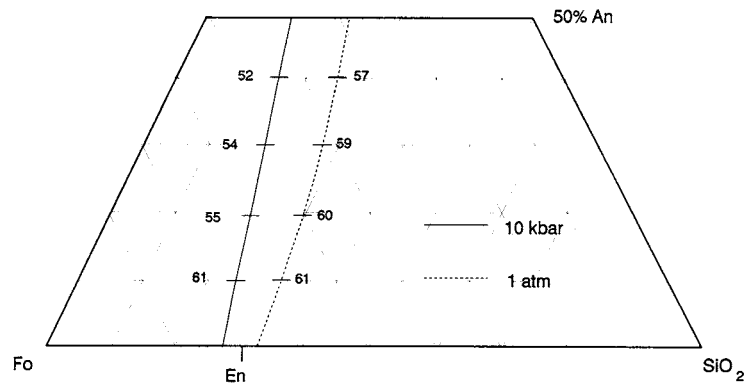

FIG. 10. Variation of SiO_2 along the olivine-pyroxene reaction curve (at one atm pressure) or cotectic (at 10 kbar) after PRESNAL et al. (1979). At 10 kbars pressure, the concentration of SiO_2 in the residual melt decreases with increasing degree of crystallization. At lower pressures, SiO_2 also decreases with crystallization but to a lesser degree. This is a possible explanation of the positive correlation between Mg# and SiO_2 in the Apollo 15 Group B green glasses.

calculated as a function of temperature and phase compositions from the results of COLSON et al. (1988) and COLSON and GUST (1989), and CaO concentrations were calculated from the results of GREEN and RINGWOOD (1973).

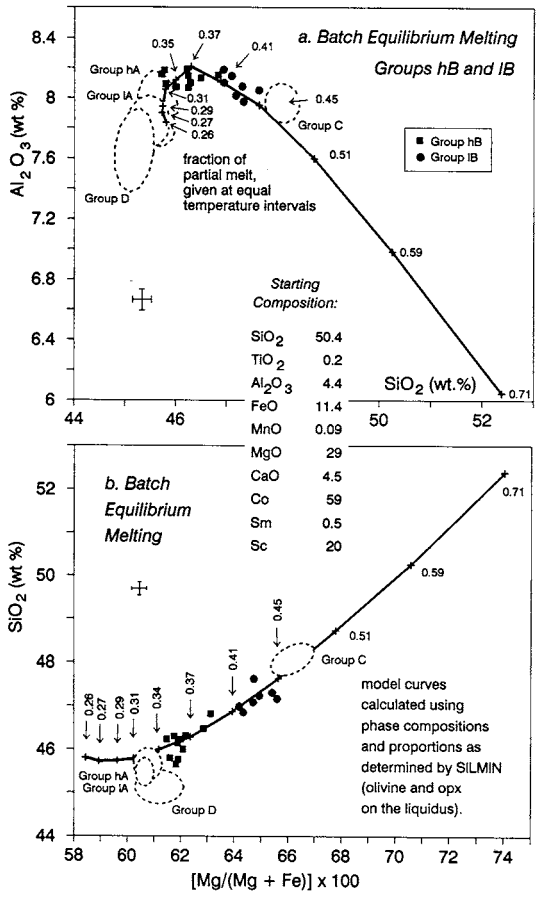

FIG. 11. Comparison of the model curve (generated in part using the SILMIN phase-equilibria program of GHIORSO et al., 1983) and the Group hB-IB compositional distribution. The major-element variation is explainable by simple batch equilibrium melting if pressure is sufficient and f_{O_2} is low enough.

When phase compositions and proportions are constrained as described above, the batch equilibrium melting model for this hypothetical source adequately describes variations in all of the major elements except CaO, including the correlation between SiO_2 and Mg# and the correlation between SiO_2 and Al_2O_3 (Fig. 11). A small amount of clinopyroxene on the liquidus would explain the CaO variation, although presence of clinopyroxene is not predicted by SILMIN. The REE concentrations and the La/Lu ratios decrease with the predicted increase in fraction melted, qualitatively as expected for such a source region.

Previous studies have concluded that partial melting with olivine and pyroxene as the residual phases cannot explain the observed trends (e.g., GROVE, 1981). We believe that conclusion is based on modelling that missed some subtle effects of changing phase compositions. Our model succeeds in explaining the Group B green glasses because it models more rigorously the phase equilibria to permit phase compositions and proportions to vary in a known way with temperature (or degree of partial melting). Phase compositions and proportions were recalculated at each degree of partial melting using SILMIN and published dependencies of partition coefficients on phase compositions and temperature. However, it is important to demonstrate that the model does not depend on some unsuspected systematic error in SILMIN and that the basic trends can be reproduced even using fixed *Kd*s for olivine and pyroxene (Fe in crystal times Mg in melt divided by Mg in crystal times Fe in melt), fixed partition coefficients, and fixed phase proportions (note that using fixed partition coefficients and *Kd*s is not the same as using fixed phase compositions). In this demonstration, *Kd* (pyroxene) = 0.316, *Kd* (olivine) = 0.357, *D* (Ca in pyroxene) = 0.22, *D* (Ca in olivine) = 0.05, *D* (Al in pyroxene) = 0.28, and *D* (Al in olivine) = 0. These values are taken from the experimental work of GREEN and RINGWOOD (1973) on the green-glass analog 12040 at 15 kbars and 1460°C. Low-Ca pyroxene/(low-Ca pyroxene + olivine) equals 0.91, taken from the experimental work of PRESNAL et al. (1979) in the Fe-free system SiO_2-An-Fo-Di at 10 kbars. The starting composition is 50.93% SiO_2, 5.04% Al_2O_3, 25.10% MgO, 13.27% FeO, and 5.16% CaO. The model curve is generated by si-

multaneously calculating all three phase compositions for various degrees of melting from 30–50%, using mass balance constraints and the equilibrium constraints given above.

The positive correlation between SiO_2 and Mg# is adequately modeled, as shown in Fig. 12. The modeled concentrations of MgO and FeO are somewhat lower and the concentrations of CaO and Al_2O_3 somewhat higher than in the group B green glasses. This is a consequence of the unrealistic constraint that bulk partition coefficients for Ca and Al are constant. Allowing partition coefficients for pyroxene to vary as a function of degree of melting (equal to the D value from GREEN and RINGWOOD (1973) times (1.5 − wt fraction melt), a variation comparable to that in the more rigorous model discussed in the preceding paragraphs) brings the concentrations of CaO, Al_2O_3, MgO, and FeO into line with those observed in the group B green glasses, while retaining the correlation between SiO_2 and Mg#. Consequently, it is reasonable to conclude that the modeling of the peculiar trends in the group B green glasses is not a consequence of some quirks of the SILMIN program.

Thus, the variation in the concentration of major and some trace elements (including Co and Sm; Fig. 9) in Groups hB and lB is predicted well by a conventional batch equilibrium melting model involving a single, essentially homogeneous source in which Co behaved as a mildly incompatible element. This model requires that the source be relatively pyroxene-rich and oxygen-poor and have high total pressure (e.g., 10–15 kbars). We have not shown this model to be unique and therefore proven. However, we have shown that processes more complex than equilibrium melting are not necessary to explain the principal compositional trends shown by Groups hB and lB.

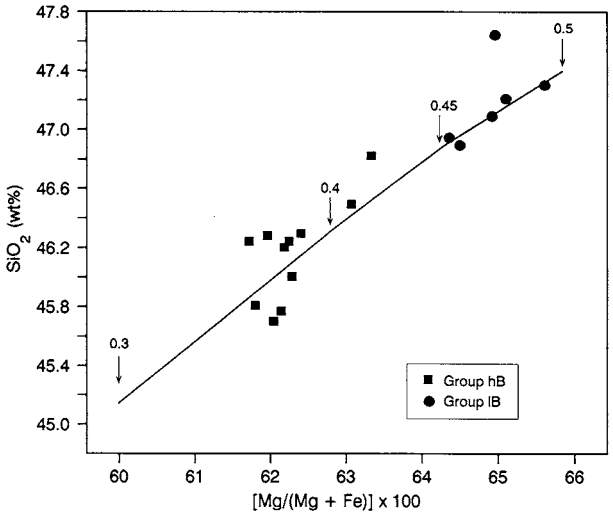

FIG. 12. Fit of model curve to the covariation of SiO_2 and Mg# for the Apollo 15 Group B green glasses analyzed in this study. This model contrasts with that shown in Fig. 11 in that SILMIN was not used to estimate phase compositions and proportions, but rather partition coefficients and equilibrium constants were fixed at values measured experimentally in Apollo 15 green-glass analog compositions at 15 kbars pressure. The fit of the curve to the data illustrates that this model does not depend on the vagaries of SILMIN. Numbers along the model curve indicate fraction melt.

Was the Group B green-glass source sufficiently poor in O_2 for Co and Ni to behave as incompatible elements? STEELE et al. (1991) estimated that at 1400°C, Ni and Co should become incompatible in pyroxene at an f_{O_2} value about 2.5 orders of magnitude below the iron-wüstite buffer. Based on the strong temperature dependence of the solubility of reduced Ni in silicate melts (COLSON, 1992), it is expected that at the higher temperatures at which the Group B green glasses formed (e.g., 1460°C; GREEN and RINGWOOD, 1973) Ni and Co should become incompatible in pyroxene at an f_{O_2} value only two orders of magnitude below the iron-wüstite buffer. If no other phase in which Ni and Co are compatible is present (such as a metal phase), the bulk partition coefficients will be less than one. This f_{O_2} value can be compared with a minimum f_{O_2} value calculated for the Group B green glasses. The minimum possible f_{O_2} value is determined at the point where FeO in the melt would reduce to form a separate metal phase, thus buffering the f_{O_2} (and causing the bulk partition coefficients to become greater than one). Taking the observed compositions of the Group B green glasses and assuming a pure Fe metal phase, the minimum f_{O_2} value calculated by use of the Fe reduction potentials reported in COLSON et al. (1990) for reduction in a pyroxene-like silicate melt is f_{O_2} = 2.7 orders of magnitude below the iron-wüstite buffer (at 1460°C). Because we presume no residual metal phase in the model discussed above, an f_{O_2} slightly above this value is required; but this minimum f_{O_2} is clearly low enough to suggest that Ni and Co could have been incompatible if no separate metal phase formed. This estimate is in contrast to the relatively high f_{O_2} value predicted by SATO (1979), based on intrinsic f_{O_2} measurements in Apollo 17 orange glass and a presumed C-CO-CO_2 buffer at depth, but is compatible with the f_{O_2} value predicted by DELANO (1990) on the basis of the high Cr concentrations in lunar picritic glasses and basalts.

Extension of the Batch Equilibrium Melting Model to Groups hA, lA, and D

Apollo 15 green-glass groups fall along boomerang-shaped curves rather than linear trends on some two-element and ratio plots (e.g., Figs. 2, 4). This complex feature has discouraged attempts to interrelate the groups to each other using models that invoke simple igneous processes. Although GROVE (1981) attempted to relate variations in Groups A and B to equilibrium formation of the phases olivine, low-Ca pyroxene, spinel, and an immiscible sulfide liquid, most researchers have explained differences between the groups as resulting from distinctly different source compositions (DELANO, 1979; MA et al., 1981). However, that the compositional groups define curves as opposed to scattering randomly has encouraged us to speculate that they may be related by some coherent igneous process rather than merely reflecting random heterogeneity in respective source regions.

The model curve for SiO_2 vs. Al_2O_3 (Fig. 11) also has a boomerang shape that roughly mimics the trend formed by Groups C, hB–lB, A, and D. This shape is a consequence of the dependence of melt composition on both element partitioning and changing phase proportions in the solid as the

degree of melting changes. For example, as the fraction of melt decreases, the proportion of Al_2O_3-rich pyroxene in the residual solid increases, causing the Al_2O_3 to become more compatible. As a result, the concentration of Al_2O_3 in the melt is maximized at the point where the tendency of incompatible Al_2O_3 to become concentrated in the melt by removal of additional solid is balanced by the increasing compatibility of Al_2O_3 in that solid.

. To test whether similar relationships can explain other intergroup alignments, we have done a mixing calculation similar to that discussed in the previous section for Groups hB and lB. However, for this exercise, we relaxed phase equilibria constraints imposed by SILMIN so that clinopyroxene would be present on the liquidus. The proportion of clinopyroxene was constrained to increase with decreasing degree of melting, as has been observed experimentally (GREEN and RINGWOOD, 1973). Partition coefficients for clinopyroxene were taken from GREEN and RINGWOOD (1973), SHIMIZU et al. (1982), and LINDSTROM (1976). We justify the inclusion of clinopyroxene in these calculations (even though SILMIN does not predict it on the liquidus) because the presence of a phase such as clinopyroxene (or garnet) is required to explain both the CaO variation in Groups hB-lB and the fact that HREEs behave less incompatibly than LREEs (Fig. 7). Also, experiments that have used a composition similar to green glass (GREEN et al., 1971; GREEN and RINGWOOD, 1973) showed that clinopyroxene is near the liquidus at a pressure of 15 kbars.

Some results of these calculations are shown in Fig. 13. Several observations are of interest. First, the shapes of the boomerang trends are modeled by simple batch equilibrium melting (other boomerang trends such as that seen in Fig. 5 and other elements, including Al_2O_3, CaO, Sc, and Yb, were also modeled successfully but are not shown). Second, the

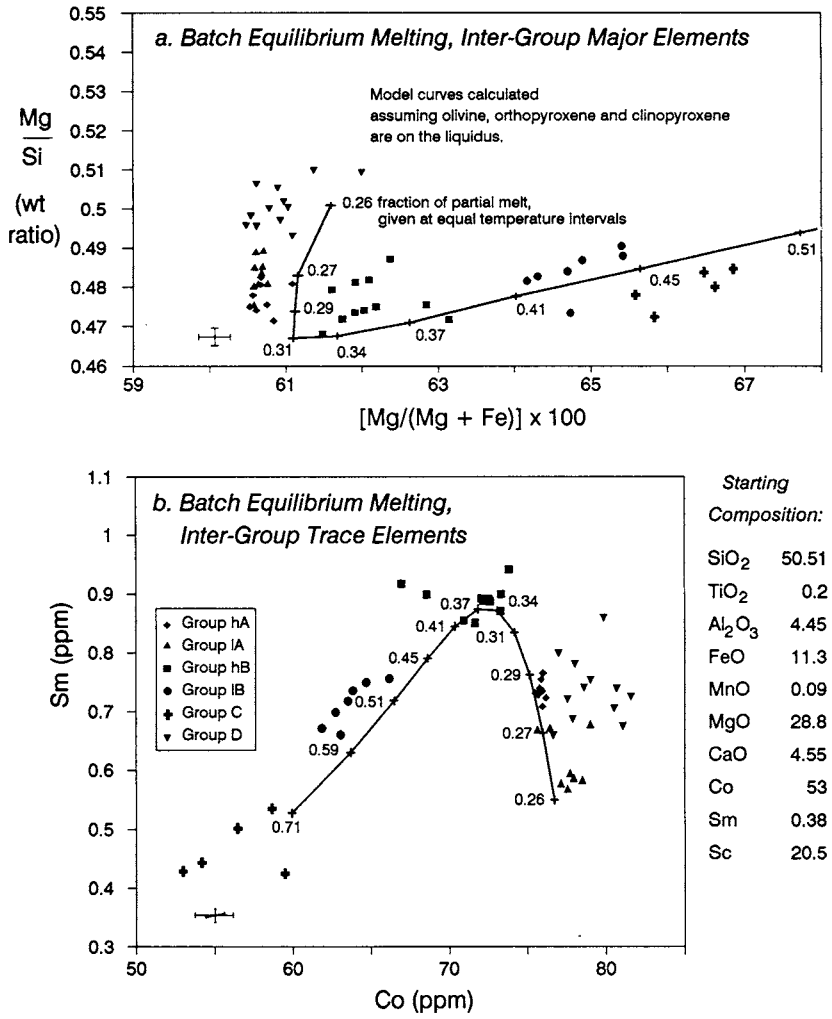

FIG. 13. Comparison of model curves for batch equilibrium melting with the green-glass compositional variation. This model explains the dominant intergroup features shown by both major and trace elements. Tick marks along the curve indicate equal temperature increments as a function of degree of melting as modeled by SILMIN for olivine + pyroxene only on the liquidus. These tick marks are closer together in regions where samples are more common, offering a possible explanation for why some compositions are more commonly sampled.

most common green-glass compositions are those that occur in a compositional range where a large change in temperature results in only a small change in melt composition (Fig. 13). Thus, this model offers a first-order explanation for why some green-glass compositions (i.e., Groups A and D) are found much more commonly than others (Groups B, C). In addition, this model reproduces qualitatively the trends in REE concentrations shown in Fig. 7. The apparently "compatible" behavior of Sm does not arise because the bulk partition coefficient for Sm becomes greater than one, but rather it is a consequence of the complex covariation of phase proportions, phase compositions, and degree of melting.

Although a model for simple batch equilibrium melting qualitatively predicts these basic features of the intergroup curves, two quantitative inconsistencies are evident in Fig. 13. First, the relative positions of Groups 1A and D are reversed between these two variation diagrams, meaning that the Group 1A concentrations of Sm and Co are modeled by a different range of melting than are the major-element concentrations in the same group. Second, the range of degree of melting required to model the Sm-Co trend is much larger than that required to model the Mg#-SiO_2 trend (or any of the major-element trends). Our calculations* suggest that these two shortcomings cannot be overcome by simple relaxation of thermodynamic constraints on the proportions of olivine, low-Ca pyroxene, and clinopyroxene entering the melts or when the source composition is unconstrained. We suggest that an equilibrium melting model that includes spinel, garnet, or other phases that may be in equilibrium with the melt and that includes consideration of additional effects on equilibrium such as adiabatic decompression of the magma during ascent may prove successful, but such modeling exceeds the scope of this paper. We note that there is scatter in the data in excess of analytical uncertainty which cannot be modeled by any smooth curve and that this scatter may be due to secondary processes.

We thus conclude that batch equilibrium melting at constant pressure and f_{O_2}, with only olivine, low-Ca pyroxene, and clinopyroxene on the liquidus, cannot explain all aspects of the compositional distribution of Apollo 15 green glass. However, it explains so much of the character of the trends, both within and between individual groups, that we believe batch equilibrium melting cannot yet be dismissed as the first-order explanation for the compositional trends shown by this suite of samples.

Green glasses comprise discrete compositional groups (Figs. 1, 2), and petrographic analysis has revealed that these groups were probably erupted during distinct eruptive episodes (STEELE, 1992). Thus, the melting described above, if it is an accurate description of green-glass petrogenesis, must have been a batch process.

* The "best fit" source composition and phase proportions were estimated using SAS (statistical analysis system), constraining each phase proportion by the arbitrary relationship $A + B \cdot X_{FeO} + C \cdot (X_{FeO})^2 + D \cdot (X_{FeO})^3$. The routine solved the mass balance equations for each element simultaneously. This is similar to a mixing program, except that the phase proportions and phase compositions were not constant.

SUMMARY

An extensive compositional survey of Apollo 15 green-glass particles indicates that the group divisions originally made by DELANO (1979) are an appropriate classification of Apollo 15 green glass, although subdivision of both Groups A and B into two groups each is warranted. The groups show statistically significant differences in the concentrations of some elements, a feature which is manifest most conspicuously by the REEs, which show differences in chondrite-normalized slopes, extent of Eu depletion, and concentrations. These groups are statistical rather than petrologic entities and thus suggest that glasses falling into compositional clusters formed in distinct events but not necessarily from different source regions or by different petrologic processes. The present study underscores the need for extremely precise analyses because small-sample obstacles such as weighing errors or analytical imprecision on the order of a few percent can impart random and correlated uncertainties of a magnitude sufficient to affect substantially interpretations of the data.

Petrogenetic modeling of Groups hB and lB using experimentally determined D values for Co and Ni suggests that batch equilibrium melting can explain the positive correlations seen between those elements and REE. Extension of this model using the SILMIN phase equilibria program indicates that this result may also hold for major elements and may also explain intergroup relationships, including boomerang shaped trends on two-element variation diagrams and why some compositional groups (e.g., A and D) are more common than others (e.g., B and C). In explaining both intra- and intergroup compositional distribution of Apollo 15 green glass, we conclude that equilibrium melting of a single, generally homogeneous source region cannot yet be dismissed.

Acknowledgments—We thank Dr. Mark Ghiorso for supplying a copy of the SILMIN program and the JSC curatorial staff for their auspicious preparation of the 15426 splits. D. Kremser is thanked for his extensive assistance with the EMP. Helpful reviews by J. W. Delano, T. L. Grove, S. S. Hughes, R. A. Schmitt, and C. K. Shearer are gratefully acknowledged. This work was supported in part by NASA grant NAG 9-56. AMS thanks the Natural Sciences and Engineering Research Council of Canada (NSERC) and Zonta International for graduate research fellowships. This work is based largely on the M. A. thesis of AMS.

Editorial handling: R. A. Schmitt

REFERENCES

ANDERS E. and EBIHARA M. (1982) Solar-system abundances of the elements. *Geochim. Cosmochim. Acta* **46**, 2363–2380.

BENCE A. E. and ALBEE A. L. (1968) Empirical correction factors for electron microanalysis of silicates and oxides. *J. Geol.* **76**, 382–403.

CAMERON K. L., DELANO J. W., BENCE A. B., and PAPIKE J. J. (1972) Petrology of the 2–4 mm sized soil fragments from Apollo 15. *The Apollo 15 Lunar Samples* (ed. J. W. CHAMBERLAIN and C. WATKINS), pp. 1–4. Lunar Sci. Inst.

CARUSI A., CAVARRETTA G., CIVITELLI G., CORADINI A., FULCHIGNONI M., FUNICIELLO R., TADDEUCCI A., and TRIGILA R. (1972) The source area of Apollo 15 "green glasses." *The Apollo*

15 Lunar Samples (ed. J. W. CHAMBERLAIN and C. WATKINS), pp. 5–9. Lunar Sci. Inst.

CAVARRETTA G., FUNICIELLO R., GILES H., NICHOLLS G. D., TADDEUCCI A., and ZUSSMAN J. (1972) Geochemistry of green glass spheres from Apollo 15 samples. *The Apollo 15 Lunar Samples* (ed. J. W. CHAMBERLAIN and C. WATKINS), pp. 202–205. Lunar Sci. Inst.

COLSON R. O. (1990) The solubility of Ni^0 in silicate melts and implication for metal/melt and crystal/melt partitioning (abstr.). *GSA Abstr. Prog.* **22,** A164.

COLSON R. O. (1992) Solubility of neutral nickel in silicate melts and implications for the Earth's siderophile element budget. *Nature* **357,** 65–68.

COLSON R. O. and GUST D. (1989) Effects of pressure on partitioning of trace elements between low-Ca pyroxene and melt. *Amer. Mineral.* **74,** 31–36.

COLSON R. O. and STEELE A. M. (1991) Major element trends in Apollo 15 green glass B. (abstr.). *Lunar Planet. Sci. XXII,* pp. 231–232.

COLSON R. O., MCKAY G. A., and TAYLOR L. A. (1988) Temperature and composition dependencies of trace element partitioning: Olivine/melt and low-Ca pyroxene/melt. *Geochim. Cosmochim. Acta* **52,** 539–553.

COLSON R. O., HASKIN L. A., and CRANE D. (1990) Electrochemistry of cations in diopsidic melt: Determining diffusion rates and redox potentials from voltammetric curves. *Geochim. Cosmochim. Acta* **54,** 3353–3367.

DAVIS J. C. (1986) *Statistics and Data Analysis in Geology.* John Wiley and Sons.

DELANO J. W. (1979) Apollo 15 green glass: Chemistry and possible origin. *Proc. 10th Lunar Planet. Sci. Conf.,* pp. 275–300.

DELANO J. W. (1986) Pristine lunar glasses: Criteria, data, and implications. *Proc. 16th Lunar Planet. Sci. Conf.; J. Geophys. Res.* **91,** D201–D213.

DELANO J. W. (1990) Experimental constraints on the oxidation state of the lunar mantle (abstr.). *Lunar Planet. Sci. XXI,* pp. 278–279.

DELANO J. W. and LINDSLEY D. H. (1982) New data on the fractionation trend in the Apollo 15 volcanic green glasses: Groups B, C (abstr.). *Lunar Planet. Sci. XXIII,* pp. 162–163.

DELANO J. W. and LIVI K. (1981) Lunar volcanic glasses and their constraints on mare petrogenesis. *Geochim. Cosmochim. Acta* **45,** 2137–2149.

EHLERS K., SISSON T. W., RECCA S. I., and GROVE T. L. (1991) The effect of oxygen fugacity of the partitioning of nickel and cobalt between olivine, silicate melt, and metal. *Geochim. Cosmochim. Acta* (submitted).

GALBREATH K. C., SHEARER C. K., PAPIKE J. J., and SHIMIZU N. (1989) An ion-microprobe study of Apollo 15 green volcanic glass: Compositional diversity and petrogenetic implications (abstr.). *GSA 1989 Ann. Mtg. Abstr. Prog.,* A284.

GALBREATH K. C., SHEARER C. K., PAPIKE J. J., and SHIMIZU N. (1990) Inter- and intra-group compositional variations in Apollo 15 pyroclastic green glass: An electron- and ion-microprobe study. *Geochim. Cosmochim. Acta* **54,** 2565–2575.

GHIORSO M. S., CARMICHAEL S. E., RIVERS M. L., and SACK R. O. (1983) The Gibbs free energy of mixing of natural silicate liquids, and expanded regular solution approximation for the calculation of magmatic intensive variables. *Contrib. Mineral. Petrol.* **84,** 107–145.

GLASS B. P. (1972) Major element composition of Apollo 15 glasses. *The Apollo 15 Lunar Samples* (ed. J. W. CHAMBERLAIN and C. WATKINS), pp. 73–77. Lunar Sci. Inst.

GREEN D. H. and RINGWOOD A. E. (1973) Significance of a primitive lunar basaltic composition present in Apollo 15 soils and breccias. *Earth Planet. Sci. Lett.* **19,** 1–8.

GREEN D. H., WARE N. G., HIBBERSON W. O., and MAJOR A. (1971) Experimental petrology of Apollo 12 basalts: Part 1, sample 12009. *Earth Planet. Sci. Lett.* **13,** 85–96.

GROVE T. L. (1981) Compositional variations among Apollo 15 green glass spheres. *Proc. Lunar Planet. Sci. Conf. 12B,* pp. 935–948.

GROVE T. L. and LINDSLEY D. H. (1978) Compositional variation and origin of lunar ultramafic green glasses (abstr.). *Lunar Planet. Sci. IX,* pp. 430–432.

HEIKEN G. H., MCKAY D. S., and BROWN R. W. (1974) Lunar deposits of possible pyroclastic origin. *Geochim. Cosmochim. Acta* **38,** 1703–1718.

HLAVA P. F., GREEN J. A., PRINZ M., NEHRU C. E., KEIL K., DOWTY E., and BUNCH T. E. (1973) Apollo 15 rake sample microbreccias and non-mare rocks: Bulk rock, mineral, and glass electron microprobe analyses. *Inst. Meteoritics Spec. Publ. No. 11.*

HUGHES S. S., DELANO J. W., and SCHMITT R. A. (1988) Apollo 15 yellow-brown volcanic glass: Chemistry and petrogenetic relations to green volcanic glass and olivine-normative mare basalts. *Geochim. Cosmochim. Acta* **52,** 2379–2391.

JAROSEWICH E., NELEN J. A., and NORBERG J. A. (1979) Electron microprobe reference samples for mineral analyses. *Smithsonian Contrib. Earth Sci.* **22,** 68–72.

JONES J. H. and DELANO J. W. (1989) A three-component model for the bulk composition of the Moon. *Geochim. Cosmochim. Acta* **53,** 513–527.

KOROTEV R. L. (1991) Geochemical stratigraphy of two regolith cores from the Central Highlands of the Moon. *Proc. 21st Lunar Planet. Sci. Conf.* pp. 229–289.

LINDSTROM D. J. (1976) Experimental study of the partitioning of the transition metals between clinopyroxene and coexisting silicate liquids. Ph.D. diss., Univ. Oregon.

LINDSTROM D. J. and KOROTEV R. L. (1982) TEABAGS: Computer programs for Instrumental Neutron Activation Analysis. *Radioanal. Chem.* **70,** 439–458.

MA M.-S., LIU Y.-G., and SCHMITT R. A. (1981) A chemical study of individual green glasses and brown glasses from 15426: Implications for their petrogenesis. *Proc. Lunar Planet. Sci. Conf. 12B,* pp. 915–933.

MCKAY D. S., CLANTON U. S., and LADLE G. (1974) Scanning electron microscope study of Apollo 15 green glass. *Proc. 4th Lunar Sci. Conf.* pp. 225–238.

NICHOLLS J. (1988) The statistics of Pearce element diagrams and the Chayes closure problem. *Contrib. Mineral. Petrol.* **99,** 11–24.

PEARCE T. H. (1978) Olivine fractionation equations for basaltic and ultrabasic liquids. *Nature* **276,** 771–774.

PEARCE T. H. (1987) The identification and assessment of spurious trends in Pearce-type ratio variation diagrams: A discussion of some statistical arguments. *Contrib. Mineral. Petrol.* **97,** 529–534.

PRESNAL D. C., DIXON J. R., O'DONNEL T. H., and DIXON S. A. (1979) Generation of mid-odean ridge tholeiites. *J. Petrol.* **20,** 3–36.

RIDLEY W. I., REID A. M., WARNER J. L., and BROWN, R. W. (1973) Apollo 15 green glass. *Phys. Earth Planet. Interiors* **7,** 133–136.

ROLLINSON H. R. and ROBERTS C. R. (1986) Ratio correlations and major element mobility in altered basalts and komatiites. *Contrib. Mineral. Petrol.* **93,** 89–97.

RUSSELL J. K. and NICHOLLS J. (1988) Analysis of petrologic hypotheses with Pearce element ratios. *Contrib. Mineral. Petrol.* **99,** 25–35.

RUSSELL J. K., NICHOLLS J., STANLEY C. R., and PEARCE T. H. (1990) Pearce element ratios: A paradigm for testing hypotheses. *Eos* **71,** 234–236, 246.

RYDER G. (1985) *Catalog of Apollo 15 Rocks.* JSC Curatorial Publ. 72, Houston, TX.

RYDER G. (1986) Analyses of Apollo 15 green glasses: Groupings and their spatial relationships (abstr.). *Lunar Planet. Sci. XVII,* pp. 738–739.

SATO M. (1979) The driving mechanism of lunar pyroclastic eruptions inferred from the oxygen fugacity behavior of Apollo 17 orange glass. *Proc. 10th Lunar Planet. Sci. Conf.* pp. 311–325.

SHEARER C. K., PAPIKE J. J., and SHIMIZU N. (1990) The relevance of picritic glasses to mare basalt volcanism. In *Abstracts for the LPI-LAPST Workshop on Mare Volcanism and Basalt Petrogenesis: "Astounding Fundamental Concepts (AFC)" Developed Over the Last Fifteen Years,* pp. 39–40. Lunar Planet. Inst.

SHIMIZU H., SANGEN K., and MASUDA A. (1982) Experimental study

on rare-earth element partitioning in olivine and clinopyroxene formed at 10 and 20 kb for basaltic systems. *Geochem. J.* **16,** 107–117.

SPUDIS P. D. and RYDER G. (1985) Geology and petrology of the Apollo 15 landing site: Past, present, and future understanding. *Eos* **66,** 721, 724–726.

STANLEY C. R. and RUSSELL J. K. (1989a) Petrologic hypothesis testing with Pearce element ratio diagrams: Derivation of diagram axes. *Contrib. Mineral. Petrol.* **103,** 78–89.

STANLEY C. R. and RUSSELL J. K. (1989b) PEARCE.PLOT: A turbo-pascal program for the analysis of rock compositions with Pearce element ratio diagrams. *Computers Geosci.* **15,** 905–926.

STANLEY C. R. and RUSSELL J. K. (1989c) PEARCE.PLOT: Interactive graphics-supported software for testing petrologic hypotheses with Pearce element-ratio diagrams. *Amer. Mineral.* **74,** 273–276.

STEELE A. M. (1992) Apollo 15 green glass: Relationships between texture and composition. *Proc. Lunar Planet. Sci. XXII,* pp. 329–341.

STEELE A. M., COLSON R. O., and HASKIN L. A. (1991) Co and Ni as incompatible elements in the lunar mantle: Implications for f_{O_2} and the petrogenesis of Apollo 15 green glass (abstr.). *Lunar Planet. Sci. XXII,* pp. 1317–1318.

STOLPER E., WALKER D., LONGHI J., and HAYES J. F. (1974) Compositional variation in lunar ultramafic glasses (abstr.). *Lunar Science V,* pp. 749–751. Lunar Sci. Inst.

WARNER J., RIDLEY W. I., REID A. M., and BROWN R. W. (1972) Apollo 15 glasses and the distribution of non-mare crustal rock types. *The Apollo 15 Lunar Samples* (ed. J. W. CHAMBERLAIN and C. WATKINS), pp. 179–181. Lunar Sci. Inst.

WOOD J. A. and RYDER G. (1977) The Apollo 15 green glass clods and the green glass enigma. (abstr.). *Lunar Sci. VIII,* pp. 1028–1028. Lunar Sci. Inst.